Volume 45
Number 1
7 January 2021
Pages 1–488

NJC

New Journal of Chemistry

A journal for new directions in chemistry

rsc.li/njc

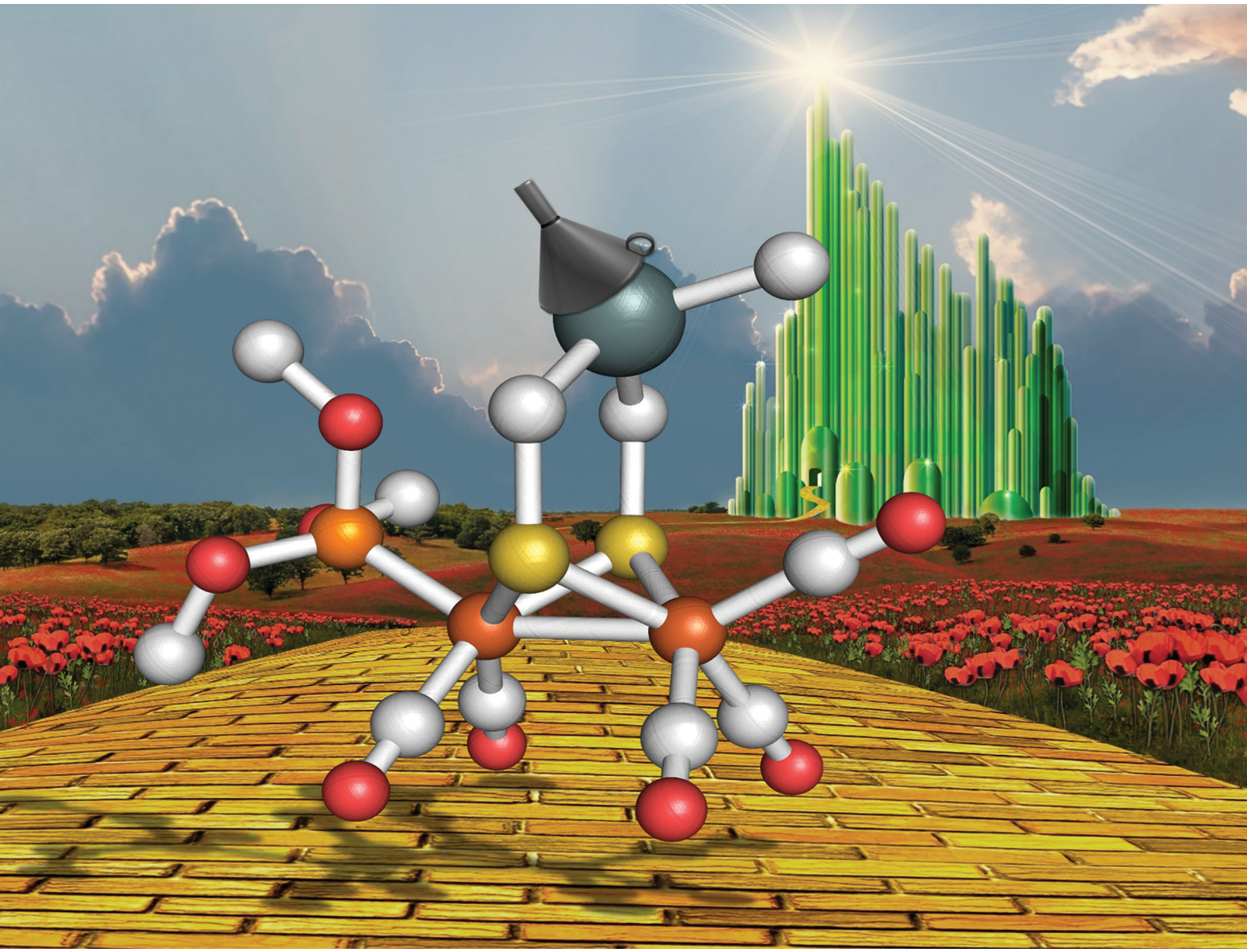

ISSN 1144-0546

ROYAL SOCIETY OF CHEMISTRY

PAPER
Hassan Abul-Futouh, Wolfgang Weigand *et al.*
Ligand effects on structural, protophilic and reductive features of stannylated dinuclear iron dithiolato complexes

cnrs

NJC

ROYAL SOCIETY OF CHEMISTRY

PAPER

View Article Online
View Journal | View Issue

Cite this: *New J. Chem.*, 2021, 45, 36

Ligand effects on structural, protophilic and reductive features of stannylated dinuclear iron dithiolato complexes†

Hassan Abul-Futouh,*[a] Laith R. Almazahreh,[bc] Sara J. Abaalkhail,[a] Helmar Görls,[c] Sven T. Stripp[d] and Wolfgang Weigand*[c]

Received 28th September 2020,
Accepted 6th November 2020

DOI: 10.1039/d0nj04790b

rsc.li/njc

The synthesis and characterization of $Fe_2(CO)_5(L)\{\mu\text{-}(SCH_2)_2SnMe_2\}$ (L = PPh_3 (**2**) and $P(OMe)_3$ (**3**)) derived from the parent hexacarbonyl complex $Fe_2(CO)_6\{\mu\text{-}(SCH_2)_2\}SnMe_2$ (**1**) are reported. Whereas **1** exhibits a unique planar structure, X-ray crystallography showed that the apical orientation of L in complexes **2** and **3** results in a chair/boat conformation of the $Fe_2S_2C_2Sn$ fused six-membered rings, which is typical for diiron dithiolato complexes. In solution, NMR and FTIR spectroscopic techniques provide evidence for a dynamic process of apical–basal site exchange of the ligand L in **2** and **3**. Protonation experiments on **2** and **3** in MeCN using CF_3CO_2H, HCl or $HBF_4{\cdot}Et_2O$ suggest enhanced protophilicity of the Fe–Fe bond due to the presence of the electron donor ligands L as well as the stannylation effect. While the carbonyl ligands in **2** stretch at lower wavenumbers ν(CO) than those in **3**, the cyclic voltammetric reduction of **2** unpredictably occurs at less negative potential than that of **3**. In contrast to **1**, the presence of PPh_3 and $P(OMe)_3$ in **2** and **3**, respectively, allows protonation prior to reduction as shown by FTIR spectroscopy and cyclic voltammetry.

Introduction

During the past two decades, considerable attention has been paid to search for viable alternatives for clean and renewable energy sources. Therefore, hydrogen has been gaining importance due to its affordability and environmental friendliness.[1–4] The high ability of [FeFe]-hydrogenases in catalyzing the production of hydrogen through reduction of protons makes their active site an interesting target for biomimetic modeling.[5–10] The active site of these enzymes, the so-called H-cluster (Fig. 1A), features a binuclear iron sub-site that is coordinated by an azadithiolato bridging moiety as well as carbon monoxide and cyanide ligands.[11–14] In addition, a canonical iron–sulfur cluster ([4Fe4S]) is linked to one iron atom through a cysteine ligand.[11–13] The reaction mechanism of H_2 oxidation and H^+ reduction at the H-cluster is under discussion.[14]

For several years, extensive efforts have been devoted to designing structural and functional models so as to mimic the protonation and redox properties of the H-cluster.[15–24] These models include a variety of dithiolato ligands, $\mu\text{-}(SCH_2)_2X$, in which the central atom/group X could be NR, CR_2, O, S, SnR_2 or (Ph)P═O (Fig. 1B).[25–39] Moreover, several research groups have reported approaches for introducing strong σ-donor ligands, such as phosphines and phosphites, at the diiron core to enhance the protophilicity of the model complexes (Fig. 1B).[40–58] In fact, multisubstituted complexes can be fully protonated affording bridging hydride (μ-H) products using strong or moderately strong acids.[55,56] In comparison, monosubstituted complexes have been little investigated in terms of protonation features. To the best of our knowledge, only one recent article has been published, which describes the protonation features of monosubstituted complexes $Fe_2(CO)_5(EPh_3)\{\mu\text{-}(SCH_2)_2\}$ (E = P, As, Sb) containing only the Fe–Fe bond as a plausible basic site.[58d] This study has shown that the addition of *ca.* 5 equiv. $HBF_4{\cdot}Et_2O$ to a solution of $Fe_2(CO)_5(EPh_3)\{\mu\text{-}(SCH_2)_2\}$ (E = P, As, Sb) in CD_2Cl_2 leads to the formation of small amount (*ca.* 5%) of bridging hydride $[Fe_2(\mu\text{-H})(CO)_5EPh_3\{\mu\text{-}(SCH_2)_2\}][BF_4]$ (E = P, As, Sb) complexes.

In our previous investigation, we have shown that the introduction of Sn atom into the dithiolato moiety of [FeFe]-hydrogenase

[a] *Department of Pharmacy, Al-Zaytoonah University of Jordan, P.O. Box 130, Amman 11733, Jordan. E-mail: h.abulfutouh@zuj.edu.jo*
[b] *ERCOSPLAN Ingenieurbüro Anlagentechnik GmbH, Arnstädter Straße 28, 99096 Erfurt, Germany*
[c] *Institut für Anorganische und Analytische Chemie, Friedrich-Schiller-Universität Jena, Humboldt Str. 8, 07743 Jena, Germany. E-mail: wolfgang.weigand@uni-jena.de*
[d] *Bioinorganic Spectroscopy, Department of Physics, Freie Universität Berlin, Arnimallee 14, 1495 Berlin, Germany*

† Electronic supplementary information (ESI) available: Crystallographic data (excluding structure factors). CCDC 2026923 for **2** and 2026924 for **3**. All NMR spectra. For ESI and crystallographic data in CIF or other electronic format see DOI: 10.1039/d0nj04790b

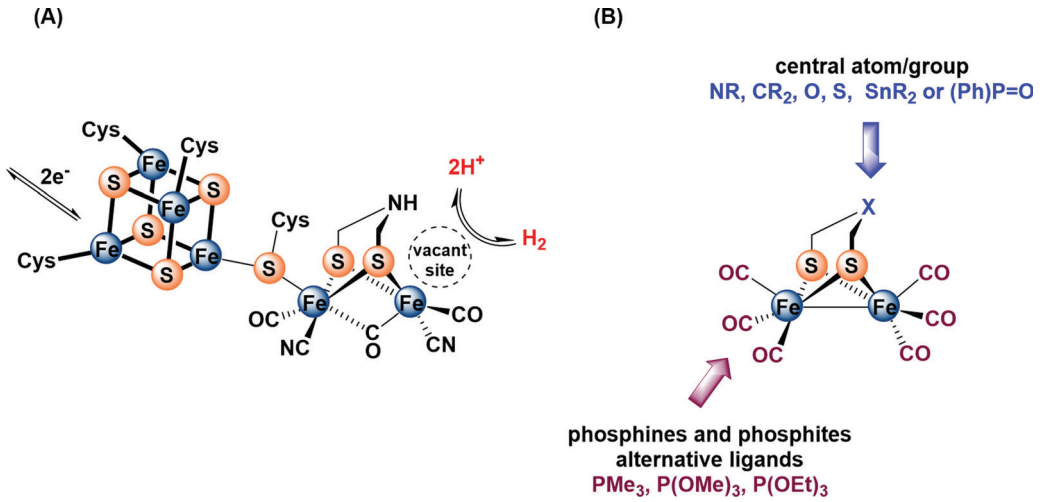

Fig. 1 (A) Structure of the H-cluster. (B) Synthetic model of the active site of [FeFe]-hydrogenase.

model complexes, *e.g.* $Fe_2(CO)_6\{\mu\text{-}(SCH_2)_2SnMe_2\}$ (**1**), increases the electron density of the μ-S atoms and the Fe–Fe bond owing to a geometry-dependent $\sigma(Sn\text{–}C) \leftrightarrow 3p(\mu\text{-}S)$ filled–filled interaction.[38] Moreover, we have revealed that further enhancement of the protophilicity of the Fe–Fe bond is established by replacing the μ-S in **1** by μ-Se, and hence the use of moderately strong CF_3CO_2H was sufficient to protonate the Fe–Fe bond.[39] In the present study, we investigate the influence of substituting one CO in **1** by stronger electron donating ligands, PPh_3 and $P(OMe)_3$, toward the protonation properties of the resulting complexes, namely $Fe_2(CO)_5(L)\{\mu\text{-}(SCH_2)_2SnMe_2\}$ (L = PPh_3 (**2**) and $P(OMe)_3$ (**3**). Herein, the synthesis and characterization as well as the molecular structures of complexes **2** and **3** are described. Furthermore, the protonation properties of the complexes have been investigated by means of IR, ^1H and $^{31}P\{^1H\}$ NMR spectroscopic techniques. The cyclic voltammetry of these complexes is employed to gain insights into reduction features in the absence and presence of acid.

Results and discussion

Synthesis and characterization

A solution of complex **1** in MeCN was treated with 1 equivalent of trimethylamine *N*-oxide ($Me_3NO{\cdot}2H_2O$) at room temperature (r.t.) for 40 minutes to afford the *in situ* acetonitrile complex *via* oxidative abstraction of CO (decarbonylation) as shown in Scheme 1.[42c] Subsequent addition of PPh_3 or $P(OMe)_3$ affords the monosubstituted complexes $Fe_2(CO)_5(L)\{\mu\text{-}(SCH_2)_2SnMe_2\}$ (L = PPh_3 (**2**) and $P(OMe)_3$ (**3**)) in moderate yields after stirring for 20 hour at r.t. (Scheme 1). Complexes **2** and **3** have been characterized by spectroscopic methods (^1H NMR, $^{13}C\{^1H\}$ NMR, $^{31}P\{^1H\}$ NMR and IR), mass spectrometry, elemental analysis, and X-ray crystallography.

The IR spectrum of **2** in MeCN displays four C≡O absorption bands, ν(CO), at 2040, 1980, 1952 and 1918 cm^{-1} while those of **3** stretch at 2045, 1990, 1972 and 1935 cm^{-1}. These frequencies are markedly shifted toward lower values relative to those of **1** (2070, 2032, 1997 and 1989 cm^{-1})[38] by an average of 49 cm^{-1} and 36 cm^{-1} for **2** and **3**, respectively. This difference in the shift of ν(CO) reflects the stronger electron donor ability of PPh_3 in comparison to $P(OMe)_3$. In comparison to **2**, the analogues complex $Fe_2(CO)_5(PPh_3)\{\mu\text{-}(SCH_2)_2CMe_2\}$ exhibits C≡O absorption bands at higher wavenumbers; ν(CO) = 2045, 1981, 1961 and 1927 cm^{-1}.[30] The disparity in the ν(CO) wavenumbers could be ascribed to an orbital interaction between the σ C–Sn bond and the S lone pair, which brings about an increased electron richness at the [2Fe2S] core.[38] The ^1H NMR spectrum of **2** exhibits two doublets (AB spin system) for the diastereotopic methylene protons centered at 1.74 ($^2J\{^1H\text{–}^1H\}$ = 12.0 Hz). In this ^1H NMR spectrum, the protons of the two CH_3 groups resonate as a singlet at 0.21 ppm with ^{119}Sn satellites ($^2J\{^{119}Sn\text{–}^1H\}$ = 27.2 Hz). Additional signals are also detected in the range of 7.67–7.43 ppm for the phenyl protons. Moreover, the diastereotopic methylene protons of **3** resonate as two doublets (AB spin system) centered at 1.74 ppm ($^2J\{^1H\text{–}^1H\}$ = 16.0 Hz). The methyl protons of the $P(OMe)_3$ ligand show a doublet at 3.76 ppm ($^3J\{^{31}P\text{–}^1H\}$ = 12.0 Hz). The ^1H NMR spectrum of **3** shows two singlets at 0.23 and 0.16 ppm with Sn satellites ($^2J\{^{119}Sn\text{–}^1H\}$ = 26.8 Hz) assigned to the CH_3 groups attributing to a slower apical–basal ligand exchange in **3** than that in **2**. Indeed, the $^{31}P\{^1H\}$ NMR spectrum (at r.t.) of **2** displays a sharp singlet at 63.52 ppm for the PPh_3 ligand while that of **3** shows a broad signal at 175.09 ppm for the $P(OMe)_3$ ligand. This observation provides also an evidence for the apical–basal site exchange such that this process is faster for the bulkier PPh_3.[30] This broadness could be explained in terms of the fluxionality of the $Fe(CO)_2P(OMe)_3$ unit such that the $P(OMe)_3$ substituent exchanges between the apical and basal positions. Upon cooling the sample to −50 °C this signal splits into singlets (182.7 and 171.0 ppm) indicating the presence of the basal and apical isomers (Fig. S7, ESI†). The $^{13}C\{^1H\}$ NMR spectra of both complexes display a singlet at 209.0 ppm for the carbonyl carbon atoms of the $Fe(CO)_3$ unit whereas those carbons in the $Fe(CO)_2P(OMe)_3$ unit resonate as a doublet centered at 211.0 ppm. Furthermore, other signals are also

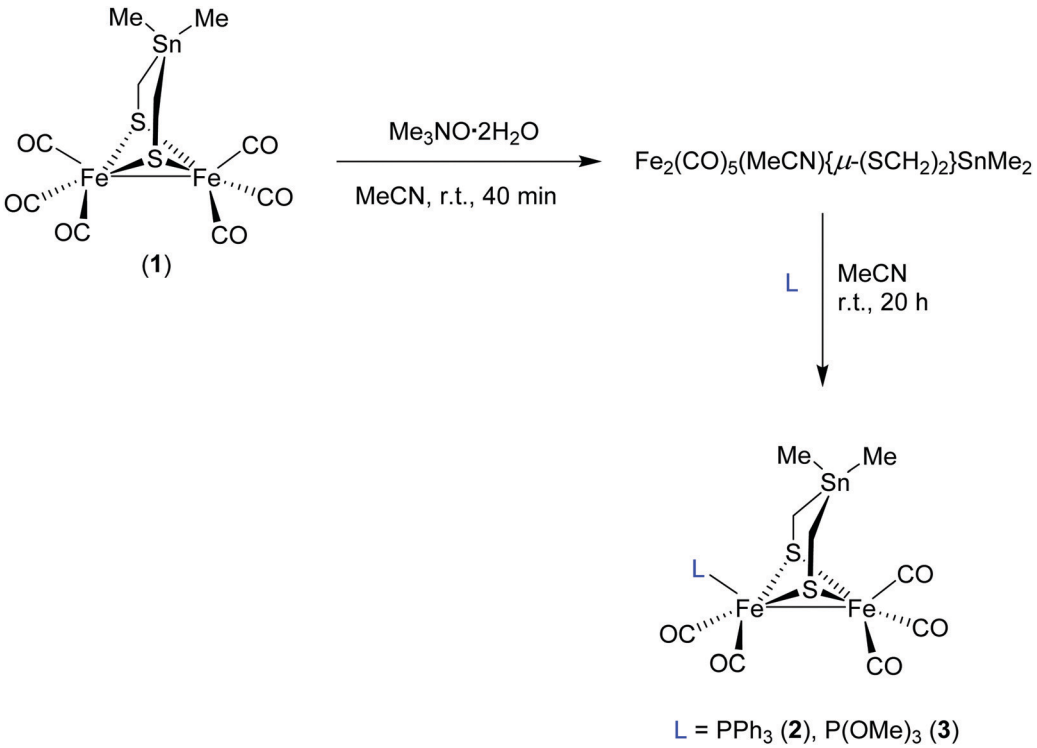

Scheme 1 Reaction pathway toward monosubstituted complexes **2** and **3**.

detected as a doublet at −6.6 and −6.8 ppm for the CH_3 group of **2** and **3**, respectively, as well as a singlet at 2.5 and 2.2 ppm for the methylene groups in **2** and **3**, respectively. The signals observed in the region of 128.5–135.5 ppm are attributed to the aromatic carbon atoms in **2** and a doublet centered at 52.2 ppm for the carbon atoms in $P(OMe)_3$ substituent of **3**.

Molecular structures

The diffusion of pentane into a CH_2Cl_2 solution of **2** or **3** at −20 °C gave suitable single crystals for X-ray diffraction studies. Fig. 2 displays the molecular structures of **2** and **3** with ellipsoids drawn at the 50% probability level.

The molecular structure of both complexes reveals the typical butterfly conformation of $[Fe_2S_2]$-cluster core (Fig. 2). In each complex, the two Fe atoms are bridged by the dithiolato $(SCH_2)_2SnMe_2$ ligand in which the bridgehead Sn atom is encircled by atoms in distorted tetrahedral fashion. The geometry of coordination around each iron center in both complexes can be best described as $Fe(CO)_3S_2$ (or $Fe(CO)_2PR_3S_2$) square pyramid, with Fe slightly positioned outside the basal plane. The angle formed from the intersection between the C_2Sn and S_2C_2 planes, so-called flap angle α, equals 146.1° or 160.3° in **2** or **3**, respectively. These angles are smaller than that found in **1** (α = 173.6°), which exhibits an almost planar S_2C_2Sn moiety (Fig. S1, ESI†).[38]

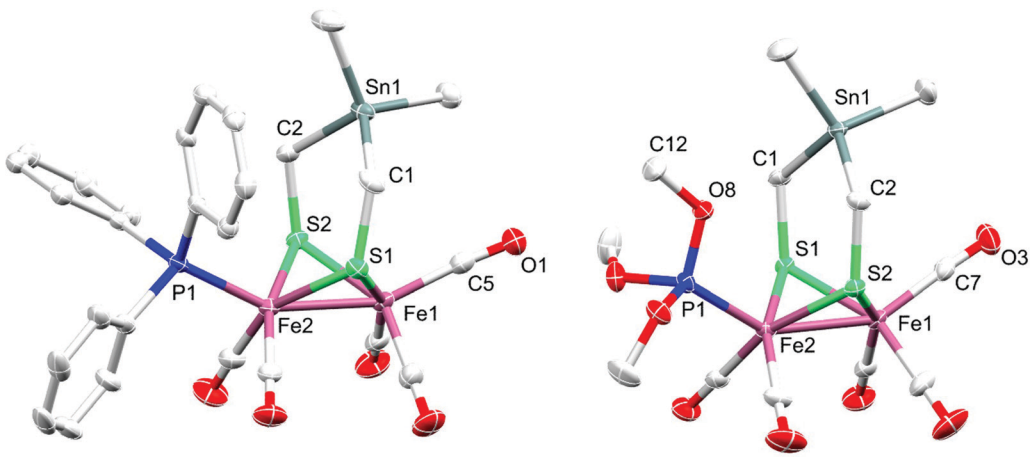

Fig. 2 Molecular structures (50% probability) of **2** (left) and **3** (right). Hydrogen atoms are omitted for clarity.

The fact that the flap angle in **3** deviates from $\alpha(\mathbf{1}) = 173.6^\circ$ more than the deviation in the case of **2** is attributed to the higher steric bulkiness of PPh_3 in comparison to that of $P(OMe)_3$. The Fe–Fe bond length in complex **2** (2.5146(4) Å) is slightly shorter than that in **1** (2.5249(5) Å), which is in turn shorter than that in **3** (2.5322(4) Å). The Fe2–P1 bond length in **2** (2.2342(6) Å) is longer than that in **3** (2.1576(6) Å), owing to the higher π-acidity of $P(OMe)_3$ compared to that of PPh_3.[59] Furthermore, the average Fe–CO bond lengths in **2** (1.78742(2) Å) and **3** (1.78898(2) Å) are slightly shorter than that in complex **1** (1.802(3) Å). These differences in Fe–CO bond lengths could be attributed to the higher Fe → CO π-backbonding in **2** or **3** than that in **1**.[38] The average Fe–S bond lengths in **2** (2.2737(6) Å) and **3** (2.2633(6) Å) are longer than that in **1** (2.2561(8) Å).[38]

Protonation study

The protophilicity of **2** and **3** towards CF_3CO_2H ($pK_a^{MeCN} = 12.65$),[60] HCl ($pK_a^{MeCN} = 10.4$)[60] and $HBF_4{\cdot}Et_2O$ ($pK_a^{MeCN} = 0.20$)[60] has been investigated by spectroscopic techniques. Complexes **2** and **3** were analyzed by attenuated total reflection Fourier-transform infrared (ATR FTIR) spectroscopy at ambient temperature and pressure. All experiments were conducted under anoxic conditions (N_2 atmosphere) and in the dark. Prior to the experiment, both complexes were dissolved in either pure MeCN and one equivalent of CF_3CO_2H, $HBF_4{\cdot}Et_2O$ or HCl. 3 μL of the solution were placed on the silicon crystal of the ATR cell and covered by a lid to minimize evaporation and protect the sample from stray light. Fig. 3 shows the FTIR absorbance spectra in the CO region (2200–1800 cm^{-1}) as well as second derivative spectra for an assignment of individual contributions. Under aprotic conditions (pure MeCN), complexes **2** and **3** show a fairly similar band pattern with a single high-frequency band around 2040 cm^{-1} and a set of three CO bands between 1990–1918 cm^{-1} (see Table 1). In protic solvent, the presence of up to 10 equiv. CF_3CO_2H or HCl did not affect the ν(CO) bands of **2** and **3**, which means that no protonation reaction took place. In the presence of 1 equiv. $HBF_4{\cdot}Et_2O$, however, complexes **2** and **3** showed mean spectral up-shifts of 82 ± 12 cm^{-1} and 22 ± 7 cm^{-1}, respectively. Despite the four-fold stronger up-shift of the CO frequencies in comparison to **3**, the spectral pattern of **2** appeared to be well conserved. Both in the presence and absence of $HBF_4{\cdot}Et_2O$, a strong band (s) is followed by another strong band with a spectral difference of ~60 cm^{-1}, a medium strong band (ms, spectral difference of ~25 cm^{-1}), and a weak band (w, spectral difference of ~35 cm^{-1}). The band pattern of **3** in protic solvent clearly differs from that of this complex in pure MeCN (Table 1).

Table 1 CO stretching frequencies of complexes **2** and **3**

Complex	Solvent	ν_{CO}/cm^{-1} (band intensity)			
2	MeCN	2040 (s)[a]	1980 (s)	1952 (ms)	1918 (w)
	$HBF_4{\cdot}Et_2O$	2112 (s)	2060 (s)	2036 (ms)	2012 (w)
	Δ	72	79	84	94
3	MeCN	2045 (s)	1990 (s)	1972 (ms)[b]	1935 (w)
	$HBF_4{\cdot}Et_2O$	2068 (s)	2015 (s)	2001 (s)	1952 (w)
	Δ	23	25	29	17

[a] The band showed a shoulder at 2028 cm^{-1}. [b] The band showed a shoulder at 1962 cm^{-1}.

In conclusion, the ATR FTIR investigation of CO band frequencies suggests protonation (or hydride formation) at complexes **2** and **3** in the presence of the strong acid $HBF_4{\cdot}Et_2O$. Analysis of the spectral region from 2600–2400 cm^{-1} indicated no specific differences for **2** and **3** between aprotic and protic solvent, which argues against sulfur protonation, at least under steady-state conditions (Fig. S2, ESI†). Indeed, this approach has been supported by testing the *in situ* protonation reactions of **2** and **3** with 1 equiv. $HBF_4{\cdot}Et_2O$ *via* ^1H and ^{31}P NMR techniques. The high-field region of the ^1H NMR spectra of **2** and **3** in the presence of $HBF_4{\cdot}Et_2O$ show typical signals due to μ-hydride species $\mathbf{2(\mu\text{-}H)^+}$ and $\mathbf{3(\mu\text{-}H)^+}$. Unfortunately, decomposition accompanies the protonation of **2**, which makes it complicated to interpret the spectra. The ^1H NMR spectrum of **3** in the presence of 1 equiv. $HBF_4{\cdot}Et_2O$ is characterized by two sets of high-field doublets at −13.9 ppm ($J\{^1H–^{31}P\}$ = 6.0 Hz) and

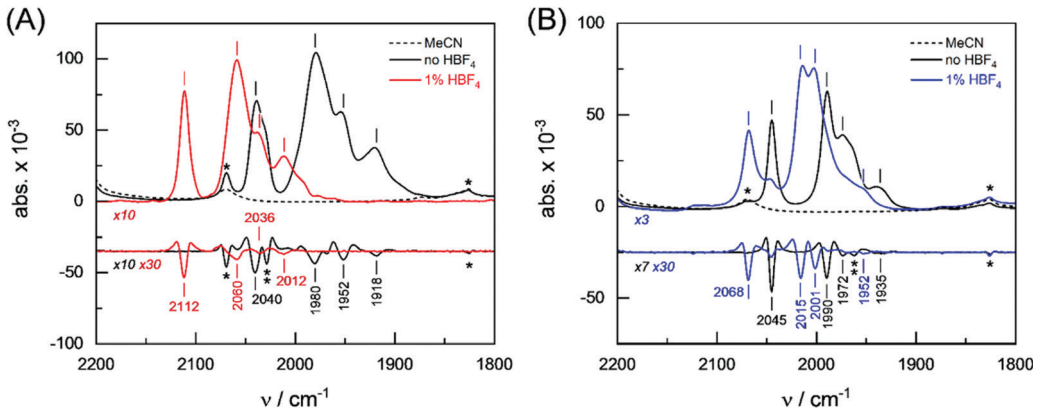

Fig. 3 FTIR absorbance spectra of complexes **2** and **3**. The CO frequency region is shown. (A) Complex **2** in solution with MeCN in the presence and absence of $HBF_4{\cdot}Et_2O$ (red and black traces) and (B) complex **3** in solution with MeCN in the presence and absence of $HBF_4{\cdot}Et_2O$ (blue and black traces). The second derivate of absorbance spectra facilitated an unambiguous frequency assignment. Asterisk: spectral contribution from MeCN. Double asterisk in (A): unassigned shoulder at 2028 cm^{-1} of the strong CO band at 2040 cm^{-1} in the absence of $HBF_4{\cdot}Et_2O$. Double asterisk in (B): unassigned shoulder at 1962 cm^{-1} of the strong CO band at 1972 cm^{-1} in the absence of $HBF_4{\cdot}Et_2O$. Dashed spectra: MeCN reference.

−14.3 ppm ($J\{^1H–^{31}P\}$ = 24.0 Hz) with *ca.* 1 : 2 relative intensity. Since the coupling between the apical PR_3 ligand and the μ-hydride is typically weak or might not be observed,[25,58d] we assign the signals at −13.9 ppm and −14.3 ppm to the apical and basal isomers, respectively. Similarly, the ^{31}P NMR spectrum of the protonated complex **3(μ-H)$^+$** displays two signals at −154.8 ppm and −145.3 ppm for the apical and basal isomers with relative intensity of *ca.* 1 : 2, respectively. Whereas $Fe_2(CO)_5EPh_3\{\mu\text{-}(SCH_2)_2\}$ (E = P, As, Sb) required excess amount of $HBF_4{\cdot}Et_2O$ to protonate the Fe–Fe bond,[58d] the presence of Sn atom in the dithiolato ligand of the complex makes the Fe–Fe bond more susceptible to protonation.

Electrochemistry

Fig. 4 shows the cyclic voltammetric reduction of **2** and **3** in comparison to that of **1** at a scan rate of 0.2 V s^{-1}. The cyclic voltammograms of **2** and **3** show irreversible cathodic peaks at E_{pc} = −1.90 V (for **2**) and E_{pc} = −2.15 V (for **3**). These reduction potentials are shifted to more negative values by 220 mV (for **2**) and 470 mV (for **3**) in comparison to that of **1** (E_{pc} = −1.68 V) due to the presence of the strong electron donating PPh_3 and $P(OMe)_3$ ligands. The less negative reduction potential of **2** compared to that of **3** is unexpected because ν(CO) wavenumbers are lower for **2**. Furthermore, this order of reduction potentials disagrees with the ligand electrochemical parameters (E_L) determined by Lever for PPh_3 (E_L = 0.39 V) and $P(OMe)_3$ (E_L = 0.42 V).[61] In contrast to **1**, increasing the scan rate achieves slight chemical reversibility for the reduction of **2** and **3** (Fig. S12–S14, ESI†), suggesting a very fast follow-up decomposition. Indeed, the enhanced chemical reversibility of the reduction of **2** at higher scan rates is accompanied with appearance of small reduction even at *ca.* −2.0 V (Fig. S12, ESI†), which might be related to reduction of the monoanionic species $\mathbf{2}^-$ into dianionic one $\mathbf{2}^{2-}$.

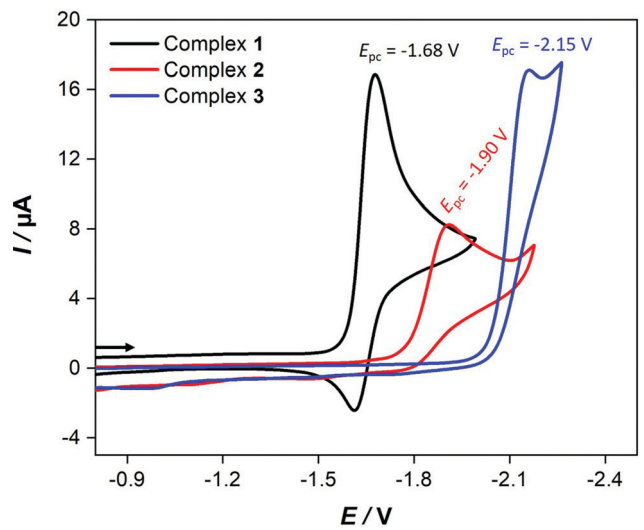

Fig. 4 Cyclic voltammetry of 1.0 mM **1–3** in CH_2Cl_2–[*n*-Bu_4N][BF_4] (0.1 M) solutions at 0.2 V s^{-1} scan rate. The arrow indicates the scan direction. The potential *E* is given in V and referenced to the Fc^+/Fc couple.

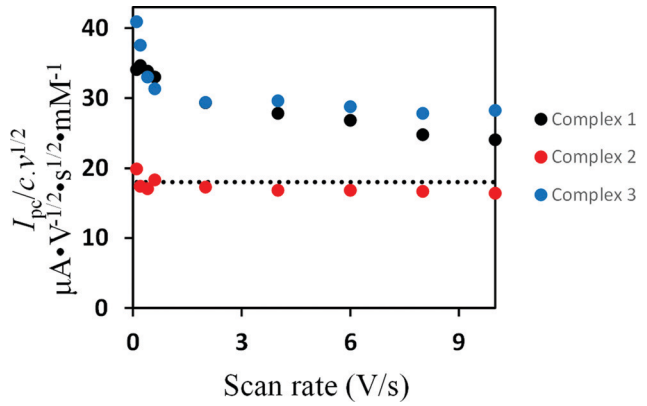

Fig. 5 The scan rates dependence of the current function of the primary reduction peaks of 1.0 mM **1–3** in CH_2Cl_2–[*n*-Bu_4N][BF_4] (0.1 M) solutions. The dashed line represents the current function expected for a one electron process assuming $D \approx 9 \times 10^{-6}$ cm^2 s^{-1}, a value calculated for various [FeFe]-hydrogenase models.

Evidence for the number of electrons involved in the reduction of the complexes could be obtained from studying the scan rate dependence of the current function $I_p/c{\cdot}\nu^{1/2}$ (I_p = peak current, *c* = concentration, ν = scan rate).[62–70] While $I_p/c{\cdot}\nu^{1/2}$ decreases towards a constant value as the scan rate increases in the cases of **1**[38] and **3**, the current function is found to be scan rate independent for **2** (Fig. 5). These observations suggest an ECE cathodic process (E = electron transfer and C = chemical process) in the case of **1** and **3** while the reduction of **2** involves simple transfer of one electron. The intervening chemical process in the ECE mechanism is suppressed by increasing the scan rate.

In the presence of $HBF_4{\cdot}Et_2O$, the cyclic voltammograms display new reduction peaks at 960 mV and 990 mV less negative potentials in comparison to the primary reduction waves of **2** and **3**, respectively, observed in the absence of acid.

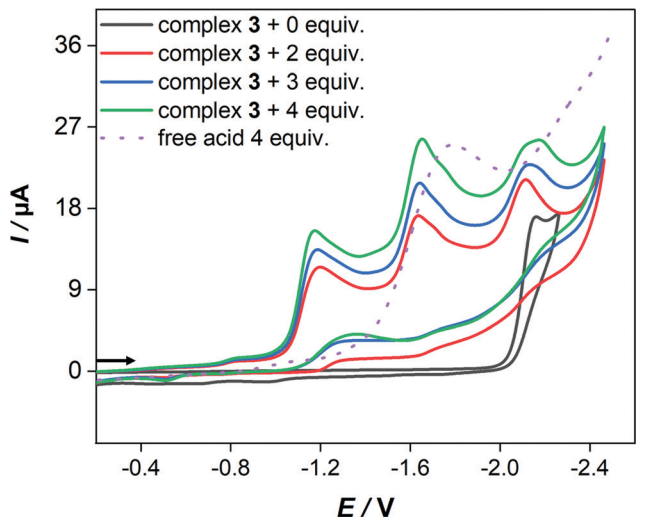

Fig. 6 Cyclic voltammetry (0.2 V s^{-1}) of 1.0 mM $Fe_2(CO)_5(P(OMe)_3)\{\mu\text{-}(SCH_2)_2\}SnMe_2$ (**3**) in CH_2Cl_2–[*n*-Bu_4N][BF_4] (0.1 M) at [$HBF_4{\cdot}Et_2O$]/[**3**] = 0–4. Potential *E* is given in volts (V) and referenced to Fc^+/Fc couple. The arrows indicate the scan direction.

These new reduction waves are attributed to the reduction of the protonated form of **2** and **3**. Similar shifts have been reported and attributed to the protonation of the Fe–Fe bond in various complexes.[55] In contrast, the presence of strong acids ($HBF_4{\cdot}Et_2O$ or CF_3SO_3H) has only led to small anodic shift of the reduction wave of **1**, which is typical thermodynamic effect resulting from protonation of the reduced species of **1**.[38] Indeed, direct reduction of $HBF_4{\cdot}Et_2O$ at the electrode is significant at high concentrations and hence the measurements were conducted only at low acid concentrations. While the cyclic voltammetry of **3** (Fig. 6) displays three distinct reduction waves (E_p = −1.17 V, −1.64 V and −2.14 V) in the presence of 2–4 equiv. $HBF_4{\cdot}Et_2O$, the situation is more complicated in the case of **2** (Fig. S15, ESI†) as an overlap of reduction waves is observed. The current of these three reduction events increases very slightly as the equiv. [$HBF_4{\cdot}Et_2O$]/[**3**] increases up to 4.

Conclusions

We have reported on the synthesis of $Fe_2(CO)_5(L)\{\mu\text{-}(SCH_2)_2\}SnMe_2$ (L = PPh_3 (**2**) and $P(OMe)_3$ (**3**)) *via* oxidative abstraction of CO from $Fe_2(CO)_6\{\mu\text{-}(SCH_2)_2\}SnMe_2$ (**1**) followed by addition of PPh_3 or $P(OMe)_3$ (Scheme 1). The variable temperature ^1H and $^{31}P\{^1H\}$ NMR spectroscopic techniques reveals the presence of two isomers of **3** at −50 °C with apically and basally oriented $P(OMe)_3$ ligand. In contrast, **2** and **3** exhibit only the apical orientation of PPh_3 or $P(OMe)_3$ in the solid state (Fig. 2). While **1** exhibits an almost planar molecular structure ($\alpha = 173.6^\circ$), the introduction of PPh_3 or $P(OMe)_3$ into the apical position in **2** or **3**, respectively, results in a deviation from planarity. The smaller flap angle measured in **3** ($\alpha = 146.1^\circ$) compared to that in the case of **2** ($\alpha = 160.3^\circ$) is attributed to the higher steric demand of the PPh_3 with respect to that of $P(OMe)_3$. Although PPh_3 is stronger electron donor ligand than $P(OMe)_3$ as evident from the ν(CO) wavenumbers of **2** and **3**, the reduction potentials of these complexes show an unexpected trend; E_{pc} = −1.90 V (for **2**) and E_{pc} = −2.15 V (for **3**). This unexpected reductive behavior might be attributed to chemical processes intervening in the electron transfer. In contrast to the case of **1**, the cyclic voltammetry of **2** or **3** show that protonation precedes electron transfer due to the presence of the strong electron donating ligands. By means of spectroscopic techniques, the protonation of **2** and **3** is proven to take place at the Fe–Fe bond leading to μ-hydride species. Only 1 equiv. of $HBF_4{\cdot}Et_2O$ is sufficient to protonate **2** and **3** at the Fe–Fe bond forming $\mathbf{2(\mu\text{-}H)^+}$ and $\mathbf{3(\mu\text{-}H)^+}$ species that is triggered not only by the presence of the PR_3 ligands, but also *via* the filled-filled interaction between the C–Sn bond and the neighboring lone pair of the μ-S atoms.

Experimental part

Materials and techniques

All reactions were performed using standard Schlenk and vacuum-line techniques under an inert gas (nitrogen). The ^1H, $^{13}C\{^1H\}$ and $^{31}P\{^1H\}$ spectra were recorded with a Bruker Avance 400 MHz spectrometer. Chemical shifts are given in parts per million with references to internal $SiMe_4$ (^1H, ^{13}C). External standard 85% H_3PO_4 was used as a reference for $^{31}P\{^1H\}$ spectral measurements. The mass spectrum was recorded with Finnigan MAT SSQ 710 instrument. Elemental analysis was performed with a Leco CHNS-932 apparatus. TLC was performed by using Merck TLC aluminum sheets (Silica gel 60 F254). Solvents from Fisher Scientific and other chemicals from Across and Aldrich were used without further purification. All solvents were dried and distilled prior to use according to standard methods. Complex **1** was synthesized according to the known literature method.[38]

Infrared spectroscopy

Fourier-transform infrared (FTIR) spectroscopy was performed in attenuated total reflection (ATR) configuration. For this, the FTIR spectrometer (Tensor27, Bruker) was equipped with a three reflections ZnSe/Si mircrocrystal (DuraDisc, Smiths Detection). All experiments were performed in a protective N_2 atmosphere, at dim light, and ambient temperatures. With 50 scans per spectrum and a scanning velocity of 80 MHz, a time resolution of 10 s was achieved that allowed probing the sample volume (1–3 μL) prior solvent evaporation. All absorbance spectra are shown as recorded (no baseline treatment or atmospheric corrections). The second derivative spectra were calculated in OPUS.

Electrochemistry

Corrections for the iR drop were performed for all experiments. Cyclic voltammetric measurements were conducted in three-electrode technique [glassy carbon disk (diameter = 1.6 mm) as working electrode, Ag/Ag^+ in MeCN as reference electrode, Pt wire as counter electrode] using a Reference 600 Potentiostat (Gamry Instruments). All experiments were performed in CH_2Cl_2 solutions (concentration of the complexes 1.0 mM) containing 0.1 M [*n*-Bu_4N][BF_4] at room temperature. The solutions were purged with N_2 and a stream of it was maintained over the solutions during the measurements. The vitreous carbon disk was polished on a felt tissue with alumina before each measurement. All potential values reported in this paper are referenced to the potential of the ferrocenium/ferrocene (Fc^+/Fc) couple.

X-ray crystal structure analysis

The intensity data for the compounds were collected on a Nonius KappaCCD diffractometer using graphite-monochromated Mo-K_α radiation. Data were corrected for Lorentz and polarization effects; absorption was taken into account on a semi-empirical basis using multiple-scans.[71–73] The structures were solved by direct methods (SHELXS)[74] and refined by full-matrix least squares techniques against Fo^2 SHELXL-2018).[75] The hydrogen atoms bonded to the methine-groups C1 and C2 of compound **3** were located by difference Fourier synthesis and refined isotropically. All other hydrogen atoms were included at calculated positions with fixed thermal parameters. All non-hydrogen atoms

were refined anisotropically.[75] MERCURY was used for structure representations.[76]

Crystal data for 2. $C_{27}H_{25}Fe_2O_5PS_2Sn$, M_r = 754.95 g mol^{-1}, red-brown prism, size 0.042 × 0.038 × 0.032 mm^3, triclinic, space group $P\bar{1}$, a = 9.7998(2), b = 10.5057(2), c = 16.7575(3) Å, α = 106.986(1), β = 91.930(1), γ = 114.973(1)°, V = 1470.99(5) Å^3, T = −140 °C, Z = 2, ρ_{calcd} = 1.704 g cm^{-3}, μ(Mo-K$_\alpha$) = 20.47 cm^{-1}, multi-scan, transmin: 0.6677, transmax: 0.7456, F(000) = 752, 9131 reflections in h(−12/12), k(−13/13), l(−21/18), measured in the range 2.272° ≤ Θ ≤ 27.362°, completeness Θ_{max} = 99.2%, 6587 independent reflections, R_{int} = 0.0142, 6284 reflections with $F_o > 4\sigma(F_o)$, 345 parameters, 0 restraints, $R1_{obs}$ = 0.0235, w$R_{obs}{}^2$ = 0.0517, $R1_{all}$ = 0.0254, w$R_{all}{}^2$ = 0.0533, GOOF = 1.070, largest difference peak and hole: 0.388/−0.491 e Å^{-3}.

Crystal data for 3. $C_{12}H_{19}Fe_2O_8PS_2Sn$, M_r = 616.75 g mol^{-1}, red-brown prism, size 0.046 × 0.042 × 0.038 mm^3, triclinic, space group $P\bar{1}$, a = 9.6675(3), b = 10.2531(3), c = 12.5768(3) Å, α = 102.077(1), β = 103.608(1), γ = 109.654(1)°, V = 1082.95(5) Å^3, T = −140 °C, Z = 2, ρ_{calcd} = 1.891 g cm^{-3}, μ(Mo-K$_\alpha$) = 27.65 cm^{-1}, multi-scan, transmin: 0.6397, transmax: 0.7456, F(000) = 608, 6883 reflections in h(−12/12), k(−13/8), l(−16/16), measured in the range 2.438° ≤ Θ ≤ 27.101°, completeness Θ_{max} = 99.2%, 4731 independent reflections, R_{int} = 0.0149, 4560 reflections with $F_o > 4\sigma(F_o)$, 256 parameters, 0 restraints, $R1_{obs}$ = 0.0200, w$R_{obs}{}^2$ = 0.0467, $R1_{all}$ = 0.0211, w$R_{all}{}^2$ = 0.0474, GOOF = 1.099, largest difference peak and hole: 0.457/−0.389 e Å^{-3}.

General procedure for the synthesis of $Fe_2(CO)_5(L)\{\mu\text{-}(SCH_2)_2SnMe_2\}$ (L = PPh_3 and $P(OMe)_3$)

To a solution of **1** in MeCN (25 mL), 2 equiv. $Me_3NO_2{\cdot}H_2O$ were added to give the respective nitrile complex within 40 min, visible by darkening of the red solution. Subsequently, 1 equiv. L was added, and the reaction mixture was stirred at r.t. for 20 h. The resulting red solution was then treatment with small amount of silica and the solvent was evaporated using vacuum transfer line. The residue was purified by column chromatography using CH_2Cl_2/hexane (1/5) as eluent. The complexes were collected from the first red-orange band and the solvent was evaporated to give the complexes as red-orange solids.

$Fe_2(CO)_5(PPh_3)\{\mu\text{-}(SCH_2)_2\}SnMe_2$ (2). Complex **1** (100 mg, 0.19 mmol) was treated with $Me_3NO_2{\cdot}H_2O$ (43 mg, 0.38 mmol) and PPh_3 (50 mg, 0.19 mmol) according to the general procedure. Yield: 68% (100 mg, 0.13 mmol). $C_{27}H_{25}Fe_2O_5PSnS_2$: C, 42.95; H, 3.34; S, 8.49. Found: C, 42.77; H, 3.41; S, 8.22. DEI-MS (m/z): 700 [M − 2CO]$^+$, 672 [M − 3CO]$^+$, 644 [M − 4CO]$^+$ and 616 [M − 5CO]$^+$. IR (MeCN): 2040(s), 1980(s), 1952(ms) and 1918(w) cm^{-1}. $^{31}P\{^1H\}$ NMR (162 MHz, $CDCl_3$): δ 63.52 (PPh_3). $^{13}C\{^1H\}$ NMR (100 MHz, $CDCl_3$): δ −6.6 (d, $J\{^{13}C\text{–}^{13}C\}$ = 36.2 Hz CH_2SnCH_3), 2.45 (CH_2SnCH_3), 128.5–135.5 (Ph) and 209.0 (CO). ^1H NMR (400 MHz, $CDCl_3$): δ 0.21 (s, 6H, $J\{Sn\text{–}^1H\}$ = 27.2 Hz, $Sn(CH_3)_2$), 1.71 (d, 2H, $J\{^1H\text{–}^1H\}$ = 8.0 Hz, CH_2Sn), 1.76 (d, 2H, $J\{^1H\text{–}^1H\}$ = 8.0 Hz, CH_2Sn) and 7.43–7.67 (m, 15H).

$Fe_2(CO)_5(P(OMe)_3)\{\mu\text{-}(SCH_2)_2\}SnMe_2$ (3). Complex **1** (100 mg, 0.19 mmol) was treated with $Me_3NO_2{\cdot}H_2O$ (43 mg, 0.38 mmol) and $P(OMe)_3$ (24 mg, 0.19 mmol) according to the general procedure. Yield: 81% (95 mg, 0.15 mmol). $C_{12}H_{19}Fe_2O_8PSnS_2$: C, 23.37; H, 3.10; S, 10.40. Found: C, 23.80; H, 3.20; S, 10.23. DEI-MS (m/z): 590 [M − CO]$^+$, 562 [M − 2CO]$^+$, 534 [M − 3CO]$^+$, 506 [M − 4CO]$^+$ and 478 [M − 5CO]$^+$ IR (MeCN): 2045(s), 1990(s), 1972(ms), 1935(w) cm^{-1}. $^{31}P\{^1H\}$ NMR (162 MHz, $CDCl_3$): δ 175.09, (298 K) (s, br, $P(OMe)_3$); 182.72, 170.99 (223 K) (2s, $P(OMe)_3$) $^{13}C\{^1H\}$ NMR (100 MHz, $CDCl_3$): δ −6.8 (d, $J\{^{13}C\text{–}^{13}C\}$ = 57.3 Hz CH_2SnCH_3), 2.2 (CH_2SnCH_3), 52.2 (d, $J\{^{31}P\text{–}^{13}C\}$ = 4.0 Hz, $P(OMe)_3$), 209.0 ($Fe(CO)_3$) and 211.0 (d, $J\{^{31}P\text{–}^{13}C\}$ = 19.0 Hz $Fe(CO)_2P(OMe)_3$). ^1H NMR (400 MHz, $CDCl_3$): δ 0.18 (s, 6H, $J\{Sn\text{–}^1H\}$ = 26.8 Hz, $Sn(CH_3)_2$), 1.65 (d, 2H $J\{^1H\text{–}^1H\}$ = 8.0 Hz, CH_2Sn), 1.78 (d, 2H, $J\{H\text{–}H\}$ = 8.0 Hz, CH_2Sn) and 3.75 (d, 9H, $J\{^1H\text{–}P\}$ = 12.0 Hz, $P(OMe)_3$).

Conflicts of interest

There are no conflicts to declare.

Acknowledgements

W. W. and H. A.-F. are thankful to Deutsche Forschungsgemeinschaft (DFG) for supporting this work (WE 1179/11-1). H. A.-F. thanks the deanship of research, Al-Zaytoonah University of Jordan for financial support (Grant No. 18/2018-2019). S. T. S. acknowledges funding through the DFG priority program 1927 (grant agreement No. 1554/5-1).

References

1 D. J. Wuebbles and A. K. Jain, *Fuel Process. Technol.*, 2001, **71**, 99.
2 S. Dunn, *Int. J. Hydrogen Energy*, 2002, **27**, 235.
3 M. Momirlan and T. N. Veziroglu, *Int. J. Hydrogen Energy*, 2005, **30**, 795.
4 S. Shima, O. Pilak, S. Vogt, M. Schick, M. S. Stagni, W. M. Klaucke, E. Warkentin, R. K. Thauer and U. Ermler, *Science*, 2008, **321**, 572.
5 J. G. Canadell, C. Le Quere, M. R. Raupach, C. B. Field, E. T. Buitenhuis, P. Ciais, T. J. Conway, N. P. Gillett, R. A. Houghton and G. Marland, *Proc. Natl. Acad. Sci. U. S. A.*, 2007, **104**, 18866.
6 M. Sensi, C. Baffert, C. Greco, G. Caserta, C. Gauquelin, L. Saujet, M. Fontecave, S. Roy, V. Artero, P. Soucaille, I. Meynial-Salles, H. Bottin, L. de Gioia, V. Fourmond, C. Léger and L. Bertini, *J. Am. Chem. Soc.*, 2016, **138**, 13612.
7 M. W. Adams, *Biochim. Biophys. Acta*, 1990, **1020**, 115.
8 M. Frey, *ChemBioChem*, 2002, **3**, 153.
9 C. Tard and C. J. Pickett, *Chem. Rev.*, 2009, **109**, 2245.
10 W. Lubitz, H. Ogata, O. Rüdiger and E. Reijerse, *Chem. Rev.*, 2014, **114**, 4081.
11 J. W. Peters, W. N. Lanzilotta, B. J. Lemon and L. C. Seefeldt, *Science*, 1998, **282**, 1853.
12 Y. Nicolet, A. L. de Lacey, X. Vernede, V. M. Fernandez, E. C. Hatchikian and J. C. Fontecilla-Camps, *J. Am. Chem. Soc.*, 2001, **123**, 1596.

13 (*a*) A. Silakov, B. Wenk, E. Reijerse and W. Lubitz, *Phys. Chem. Chem. Phys.*, 2009, **11**, 6592; (*b*) G. Berggren, A. Adamska, C. Lambertz, T. R. Simmons, J. Esselborn, M. Atta, S. Gambarelli, J. M. Mouesca, E. Reijerse, W. Lubitz, T. Happe, V. Artero and M. Fontecave, *Nature*, 2013, **499**, 66.
14 (*a*) M. Haumann and S. T. Stripp, *Acc. Chem. Res.*, 2018, **51**, 1755; (*b*) H. Land, M. Senger, G. Berggren and S. T. Stripp, *ACS Catal.*, 2020, **10**, 7069.
15 Y. Li and T. B. Rauchfuss, *Chem. Rev.*, 2016, **116**, 7043.
16 T. R. Simmons, G. Berggren, M. Bacchi, M. Fontecave and V. Artero, *Coord. Chem. Rev.*, 2014, **270–271**, 127.
17 S. Gao, Y. Liu, Y. Shao, D. Jiang and Q. Duan, *Coord. Chem. Rev.*, 2020, **402**, 213081.
18 W. Lubitz, H. Ogata, O. Rüdiger and E. Reijerse, *Chem. Rev.*, 2014, **114**, 4081.
19 H. Abul-Futouh, L. R. Almazahreh, M. K. Harb, H. Görls, M. El-khateeb and W. Weigand, *Inorg. Chem.*, 2017, **56**, 10437.
20 H. Abul-Futouh, A. Q. Daraosheh, J. Windhager, H. Görls and W. Weigand, *Polyhedron*, 2019, **174**, 114155.
21 J. D. Lawrence, H. Li, T. B. Rauchfuss, M. Bénard and M. Rohmer, *Angew. Chem., Int. Ed.*, 2001, **40**, 1768.
22 M. Watanabe, K. Goto, T. Miyazaki, M. Shibahara, Y. J. Chang, T. J. Chow and T. Ishihara, *New J. Chem.*, 2019, **43**, 13810.
23 H. Abul-Futouh, A. Skabeev, D. Botteri, Y. Zagranyarski, H. Görls, W. Weigand and K. Peneva, *Organometallics*, 2018, **37**, 3278.
24 H. Abul-Futouh, Y. Zagranyarski, C. Müller, M. Schulz, S. Kupfer, H. Görls, M. El-khateeb, S. Gräfe, B. Dietzek, K. Peneva and W. Weigand, *Dalton Trans.*, 2017, **46**, 11180.
25 M. E. Carroll, B. E. Barton, T. B. Rauchfuss and P. J. Carroll, *J. Am. Chem. Soc.*, 2012, **134**, 18843.
26 J. Hou, X. Peng, J. Liu, Y. Gao, X. Zhao, S. Gao and K. Han, *Eur. J. Inorg. Chem.*, 2006, 4679.
27 W.-G. Wang, H.-Y. Wang, G. Si, C.-H. Tung and L.-Z. Wu, *Dalton Trans.*, 2009, 2712.
28 Y. Si, C. Ma, M. Hu, H. Chen, C. Chen and Q. Liu, *New J. Chem.*, 2007, **31**, 1448.
29 R. Zaffaroni, T. B. Rauchfuss, D. L. Gray, L. De Goia and G. Zampelli, *J. Am. Chem. Soc.*, 2012, **134**, 19260.
30 M. L. Singleton, R. M. Jenkins, C. L. Klemashevich and M. Y. Darensbourg, *C. R. Chim.*, 2008, **11**, 861.
31 B. E. Barton, M. T. Olsen and T. B. Rauchfuss, *J. Am. Chem. Soc.*, 2008, **130**, 16834.
32 H. X. Li and T. B. Rauchfuss, *J. Am. Chem. Soc.*, 2002, **124**, 726.
33 L.-C. Song, Z.-Y. Yang, H.-Z. Bian, Y. Liu, H.-T. Wang, X.-F. Liu and Q.-M. Hu, *Organometallics*, 2005, **24**, 6126.
34 L.-C. Song, Z.-Y. Yang, Y.-J. Hua, H.-T. Wang, Y. Liu and Q.-M. Hu, *Organometallics*, 2007, **26**, 2106.
35 J. Windhager, M. Rudolph, S. Brautigam, H. Görls and W. Weigand, *Eur. J. Inorg. Chem.*, 2007, 2748.
36 L.-C. Song, A.-G. Zhu and Y.-Q. Guo, *Dalton Trans.*, 2016, **45**, 5021.
37 L. R. Almazahreh, U.-P. Apfel, W. Imhof, M. Rudolph, H. Görls, J. Talarmin, P. Schollhammer, M. El-khateeb and W. Weigand, *Organometallics*, 2013, **32**, 4523.
38 H. Abul-Futouh, L. R. Almazahreh, T. Sakamoto, N. Y. T. Stessman, D. L. Lichtenberger, R. S. Glass, H. Görls, M. El-khateeb, P. Schollhammer, G. Mloston and W. Weigand, *Chem. – Eur. J.*, 2017, **23**, 346.
39 H. Abul-Futouh, M. El-khateeb, H. Görls, K. J. Asali and W. Weigand, *Dalton Trans.*, 2017, **4**, 2937.
40 L. Duan, M. Wang, P. Li, Y. Na, N. Wang and L. Sun, *Dalton Trans.*, 2007, 1277.
41 L.-C. Song, Z.-Y. Yang, H.-Z. Bian, Y. Liu, H.-T. Wang, X.-F. Liu and Q.-M. Hu, *Organometallics*, 2005, **24**, 6126.
42 (*a*) C. M. Thomas, O. Rudiger, T. Liu, C. E. Carson, M. B. Hall and M. Y. Darensbourg, *Organometallics*, 2007, **26**, 3976; (*b*) L. R. Almazahreh, W. Imhof, J. Talarmin, P. Schollhammer, H. Görls, M. El-khateeb and W. Weigand, *Dalton Trans.*, 2015, **44**, 7177; (*c*) J. Windhager, U.-P. Apfel, T. Yoshino, N. Nakata, H. Görls, M. Rudolph, A. Ishii and W. Weigand, *Chem. – Asian J.*, 2010, **5**, 1600.
43 P. Li, M. Wang, C. He, X. Liu, K. Jin and L. Sun, *Eur. J. Inorg. Chem.*, 2007, 3718.
44 W. Gao, J. Ekstrom, J. Liu, C. Chen, L. Eriksson, L. Weng, B. Åkermark and L. Sun, *Inorg. Chem.*, 2007, **46**, 1981.
45 A. Jablonskytė, J. A. Wright and C. J. Pickett, *Eur. J. Inorg. Chem.*, 2011, 1033.
46 Y.-C. Liu, C.-H. Lee, G.-H. Lee and M.-H. Chiang, *Eur. J. Inorg. Chem.*, 2011, 1155.
47 H. Abul-Futouh, H. Görls and W. Weigand, *Z. Anorg. Allg. Chem.*, 2017, **643**, 1615.
48 A. Q. Daraosheh, H. Abul-Futouh, H. Görls and W. Weigand, *Inorg. Chim. Acta*, 2020, **503**, 119377.
49 F. Gloaguen, J. D. Lawrence, M. Schmidt, S. R. Wilson and T. B. Rauchfuss, *J. Am. Chem. Soc.*, 2001, **123**, 12518.
50 C. M. Thomas, T. Liu, M. B. Hall and M. Y. Darensbourg, *Inorg. Chem.*, 2008, **47**, 7009.
51 S. Pullen, S. Maji, M. Stein and S. Ott, *Dalton Trans.*, 2019, **48**, 5933.
52 Z. Wang, J. He, S. Lü, W.-D. Jiang, Y. Wu, J. Jiang, Y. Xie, C. Mu, A. Li, Y.-L. Li and Q.-L. Li, *Appl. Organomet. Chem.*, 2019, **33**, e5184.
53 M.-Y. Hu, P.-H. Zhao, J.-R. Li, X.-L. Gu, X.-B. Jing and X.-F. Liu, *Appl. Organomet. Chem.*, 2020, **34**, e5523.
54 H.-M. Lin, J.-R. Li, C. Mu, A. Li, X.-F. Liu, P.-H. Zhao, Y.-L. Li, Z.-Q. Jiang and H.-K. Wu, *Appl. Organomet. Chem.*, 2019, **33**, e5196.
55 S. Tschierlei, S. Ott and R. Lomoth, *Energy Environ. Sci.*, 2011, **4**, 2340.
56 N. Wang, M. Wang, L. Chen and L. Sun, *Dalton Trans.*, 2013, **42**, 12059.
57 K. Fauvel, R. Mathieu and R. Poilblanc, *Inorg. Chem.*, 1976, **15**, 976.
58 (*a*) A. Jablonskyte, J. A. Wright and C. J. Pickett, *Dalton Trans.*, 2010, **39**, 3026; (*b*) X. Zhao, I. P. Georgakaki, M. L. Miller, R. Mejia-Rodriguez, C.-Y. Chiang and M. Y. Darensbourg, *Inorg. Chem.*, 2002, **41**, 3917; (*c*) X. Zhao, Y.-M. Hsiao,

C.-H. Lai, J. H. Reibenspies and M. Y. Darensbourg, *Inorg. Chem.*, 2002, **41**, 699; (*d*) S. Ghosh, A. Rahaman, G. Orton, G. Gregori, M. Bernat, U. Kulsume, N. Hollingsworth, K. B. Holt, S. E. Kabir and G. Hogarth, *Eur. J. Inorg. Chem.*, 2019, 4506; (*e*) J.-R. Li, M.-Y. Hu, S. Lü, X.-L. Gu, X.-B. Jing and P.-H. Zhao, *Appl. Organomet. Chem.*, 2020, **34**, e5929.

59 W. Lin Su, P. H. Huang, W.-T. Chen, W.-Y. Hsu, H.-Y. Chang, S.-Y. Ho, S.-P. Wanga and S.-G. Shyu, *J. Chin. Chem. Soc.*, 2011, **58**, 163.

60 R. H. Morris, *Chem. Rev.*, 2016, **116**, 8588.

61 A. B. P. Lever, *Inorg. Chem.*, 1990, **29**, 1271.

62 L. Schwartz, P. S. Singh, L. Eriksson, R. Lomoth and S. Ott, *C. R. Chim*, 2008, **11**, 875.

63 J. Chen, A. K. Vannucci, C. A. Mebi, N. Okumura, S. C. Borowski, M. Swenson, L. T. Lockett, D. H. Evans, R. S. Glass and D. L. Lichtenberger, *Organometallics*, 2010, **29**, 5330.

64 S. P. Best, S. J. Borg, J. M. White, M. Razavet and C. J. Pickett, *Chem. Commun.*, 2007, 4348.

65 F. Gloaguen and T. B. Rauchfuss, *Chem. Soc. Rev.*, 2009, **38**, 100.

66 H. Abul-Futouh, M. El-khateeb, H. Görls and W. Weigand, *Heteroat. Chem.*, 2018, **29**, e21446.

67 G. Qian, W. Zhong, Z. Wei, H. Wang, Z. Xiao, L. Long and X. Liu, *New J. Chem.*, 2015, **39**, 9752.

68 R. S. Nicholson and I. Shain, *Anal. Chem.*, 1965, **37**, 178.

69 M. K. Harb, H. Alshurafa, M. El-khateeb, A. Al-Zuheiri, H. Görls, H. Abul-Futouh and W. Weigand, *ChemistrySelect*, 2018, **3**, 8867.

70 R. Trautwein, H. Abul-Futouh, H. Görls, W. Imhof, L. R. Almazahreh and W. Weigand, *New J. Chem.*, 2019, **43**, 12580.

71 COLLECT, Data Collection Software, Nonius B.V., Netherlands, 1998.

72 Z. Otwinowski and W. Minor, Processing of X-Ray Diffraction Data Collected in Oscillation Mode, in *Macromolecular Crystallography, Part A*, ed. C. W. Carter and R. M. Sweet, Methods in Enzymology, Academic Press, San Diego, USA, 1997, vol. 276, p. 307.

73 L. Krause, R. Herbst-Irmer, G. M. Sheldrick and D. Stalke, *J. Appl. Crystallogr.*, 2015, **48**, 3.

74 G. M. Sheldrick, *Acta Crystallogr., Sect. A: Found. Crystallogr.*, 2008, **64**, 112.

75 G. M. Sheldrick, *Acta Crystallogr., Sect. C: Struct. Chem.*, 2015, **71**, 3.

76 C. F. Macrae, P. R. Edgington, P. McCabe, E. Pidcock, G. P. Shields, R. Taylor, M. Towler and J. van de Streek, *J. Appl. Crystallogr.*, 2006, **39**, 453.

